AN ANALYSIS OF THE KALMAN FILTER IN THE GAMMA RAY OBSERVATORY (GRO) ONBOARD ATTITUDE DETERMINATION SUBSYSTEM

Frank Snow and Richard Harman
Code 554/Flight Dynamics Analysis Branch

Joseph Garrick
Code 552/Flight Dynamics Software Development Branch
Goddard Space Flight Center
Greenbelt, Maryland

ABSTRACT

The Gamma Ray Observatory (GRO) spacecraft needs a highly accurate attitude knowledge to achieve its mission objectives. Utilizing the fixed-head star trackers (FHSTs) for observations and gyroscopes for attitude propagation, the discrete Kalman Filter processes the attitude data to obtain an onboard accuracy of 86 arc seconds (3 sigma).

A combination of linear analysis and simulations using the GRO Software Simulator (GROSS) are employed to investigate the Kalman filter for stability and the effects of corrupted observations (misalignment, noise), incomplete dynamic modeling, and nonlinear errors on the Kalman filter. In the simulations, on-board attitude is compared with true attitude, the sensitivity of attitude error to model errors is graphed, and a statistical analysis is performed on the residuals of the Kalman Filter. In this paper, the modeling and sensor errors that degrade the Kalman filter solution beyond mission requirements are studied, and methods are offered to identify the source of these errors.

1. GAMMA RAY OBSERVATORY

The Gamma Ray Observatory (GRO) is a three-axis stabilized spacecraft scheduled to be launched in 1990 by the Space Transportation System (STS). The GRO science instruments study gamma ray sources between 0.1 and 30000 megaelectronvolts (MeV) before they are absorbed by the Earth's atmosphere. The spacecraft is designed to stay inertially pointed, using reaction wheel control, for 2 weeks at a time before maneuvering to the next gamma ray target. The nominal spacecraft orbit will be 350- to 450-kilometer altitude, 0.0001 eccentricity, and 28.5 degrees (deg) inclination.

GRO is equipped with two National Aeronautics and Space Administration (NASA) standard onboard computers (OBCs) of which one is used as a backup. The OBC performs sensor data processing and actuator commanding. There are five OBC control modes: Standby Mode (SM), Normal Pointing Mode (NPM), Normal Maneuver Mode (NMM), Thruster Maneuver Mode (TMM), and Velocity Control Mode (VCM). The NPM is the gamma ray inertial pointing mode.

GRO has an onboard attitude determination accuracy requirement of 86.4 arc seconds per axis (arc-sec) (3 sigma) during the normal science observation mode. This accuracy is accomplished by the use of two fixed-head star trackers (FHSTs) and an inertial reference unit (IRU). Both of these attitude sensors have been used on the Solar Maximum Mission (SMM), Landsat-4, and Landsat-5 spacecraft. The attitude is propagated using the IRU data and updated after a FHST measurement by using a Kalman filter.

1.1 FHST DESCRIPTION

The FHST is an attitude sensor that searches for, detects, and tracks stars; provides accurate position and intensity information on stars in its field of view (FOV); and generates status flags and parameters that characterize the sensor operation.

When light from the star enters the optical lens, the image of the star is focused on the photocathode of an image dissector tube (IDT), which magnetically deflects and focuses the electrons onto an aperture in a plate. The corresponding signal is amplified and processed to provide intensity and position information. The FHST functions in two operational modes: search and track mode.

In the total field of view (TFOV), a search mode consists of a horizontal scan pattern with appropriate vertical shifts at the ends (raster). Four commandable thresholds set the minimum sensitivity for acquiring a star. Position and intensity output during the search mode do not convey meaningful information.

When a star is acquired, the detector traces a small cross pattern in the form of a figure 8 centered on the star image. A star present flag is set to indicate that star position and intensity data are valid for the tracked star. The track pattern remains locked on the star during attitude changes. If the star leaves the TFOV, if its intensity falls below the commanded threshold, or if a break-track command is received, search mode resumes.

With the optional offset mode capability, a small offset raster scan can be commanded in a reduced field of view (RFOV). If a star is acquired, it will be tracked throughout the TFOV. If the star is lost, a reduced scan will begin at the original position in the RFOV. FHST parameters and values are listed in Table 1.

1.2 IRU Description

The IRU is an attitude sensor consisting of a gyro package that measures inertial vehicle rates about the sensor axis. Output consists of analog rates, accumulated angles, range status, and temperature.

The IRU contains three spinning wheels or rotors. Each rotor is mounted on two gimbals to provide 2 degrees of freedom and, therefore, rate information along two body axes (two-channel output). The

Table 1. FHST Parameters and Values

Parameter	Value
TFOV	8 by 8 deg
RFOV	1.5 by 1.5 deg
Range of star visual magnitude	+5.7 to -7.0
Number of threshold settings	4
Maximum tolerable vehicle rate	0.3 deg/second (sec)
Search mode:	
Scan type	Raster
Number of lines in TFOV	70
Maximum acquisition time	10 sec (TFOV), 1.5 sec (RFOV)
Track mode:	
Scan type	Unidirectional cross-scan
Scan period	100 milliseconds
Output rate	10/sec (each axis)
Accuracy	10/arc-sec (1 sigma) calibrated over 8-deg diameter circular FOV
Nominal data resolution	7 arc-sec

six-channel IRU configuration provides dual redundancy along each body axis. The IRU assembly is fixed in the spacecraft (strapdown). The current required to magnetically torque a gimbal to maintain null deflection (torque rebalancing) is proportional to the accumulated rotation angle (rate integrating) about the corresponding body axis. Torque current is differenced after small intervals of time to generate analog rates. The IRU can operate in either high-rate or low-rate mode (range status). IRU parameters and values are listed in Table 2.

Table 2. IRU Parameters and Values

Parameter	Value
Scale factor stability	±0.01 percent/month (low rate) ±0.1 percent/month (high rate)
Acceleration-insensitive drift rate (AIDR)	±0.04 arc-sec/sec for 30 days of start-stop operation (low rate), ±0.003 arc-sec/sec for 6 hours of continuous operation (low rate), ±0.001 deg/sec for 30 days (high rate)
Nominal data resolution	0.8 arc-sec/count (high rate), 0.05 arc-sec/count (low rate)
High-rate range	±2.0 deg/sec
Low-rate range	±400 arc-sec/sec

1.3 KALMAN FILTER

A Kalman filter combines all available measurement data, plus prior knowledge about the system and measuring devices, to produce an estimate of the state vector such that the error is statistically minimized. The Kalman filter of the GRO flight software uses the error state space formulation method in which the state vector contains the errors in the spacecraft attitude and the gyroscope biases. The state vector is updated whenever there is a measurement by the FHSTs or the fine Sun sensor (FSS).

From the dynamic modeling of the state vector, the Kalman filter computes a noise covariance matrix and then propagates the state covariance matrix from the last filter update. Propagation of this covariance matrix requires the computation of the state transition matrix for the dynamic equations. After propagation of the covariance matrix, the Kalman filter uses the measurement model and the propagated covariance matrix to compute the Kalman gain matrix. From this gain matrix and the measurement residuals, the Kalman filter computes the updated state vector to correct the attitude and gyro drift biases. The last processing in the Kalman filter is to update the covariance matrix to reflect the effects of sensor measurement processing.

2. GRO SOFTWARE SIMULATOR

The primary tool used in this analysis was the GRO Software Simulator (GROSS) developed in the Flight Dynamics Division. GROSS is a closed-loop GRO Attitude Control System (ACS) simulator, which for this analysis consisted of two major functions: the Truth Model (TM) and the functional OBC.

The TM models spacecraft dynamics, environmental torques, and hardware. The environmental models take into account four torques that act to perturb the dynamics. These are the solar radiation, residual magnetic dipole, aerodynamic, and gravity gradient torques. The hardware model reflects a detailed functional description of the actuators, sensors, and moving parts. These models include not only nominal performance, but also biases, noises, misalignments, and failures. The actuators modeled include four reaction wheels, eight attitude control thrusters (ACTs), four orbit adjust thrusters (OATs), and two magnetic torquer assemblies (MTAs). The sensors modeled include two (FSSs), four coarse Sun sensors (CSSs), four reaction wheel tachometers, two FHSTs, an IRU consisting of three gyros and dual-output capabilities per axis, and two three-axis magnetometers (TAMs). The moving parts are the High-Gain Antenna (HGA) and solar arrays, which respond to ground pointing commands. The movement of these create a momentum component to be used in the dynamics. The dynamics modeling uses a fourth-order, variable-step, Adams-Moulton-Bashforth (AMB) numerical integrator.

The functional OBC is GROSS's FORTRAN representation of GRO's onboard flight software. The OBC processes sensor data from the TM, determines the spacecraft attitude, and generates the appropriate control commands based on the control laws for the current mode. The functional OBC and the GRO attitude flight software were coded from the same software specifications. In an attempt to model the spacecraft flight software as closely as possible, the functional OBC executes the same algorithms including the same approximations for trigonometric functions. The Attitude Estimation function in the GROSS OBC is shown in Figure 1.

2.1 GROSS MODELING OF FHST

The FHST model generates the star camera data. The camera is commanded by the OBC to search an RFOV for a guide star. Once a star is acquired by the FHST, and it meets the prescribed restraints, the star is tracked. Output from a star tracker consists of a (u, v) coordinate measured in the camera's focal plane, along with the star's intensity. The camera will continue to track the star until a break-track command is received from the OBC or from the ground, or until the star proceeds to exit the TFOV.

GROSS simulates the search mode by ordering the stars found in the RFOVs associated with the current pointing in the same fashion as would be encountered in a normal search mode. When a star is determined to be the guide star for that RFOV by the OBC, the FHST will hold on that star and do all the processing in the model with this star's position and intensity data. The FHST model will also determine if the line of sight (LOS) is occulted by the Earth, Sun, or Moon and will take the appropriated action by closing the shutter and issuing the appropriate status flag to the OBC, indicating that it is currently inhibited. After the true data are generated, the FHST model will employ a decalibration scheme to corrupt the values sent to the OBC.

In the OBC, the FHST processing routine uses a calibration scheme to correct for temperature, flat field, magnetic fields, and star intensity variations.

GROSS provides the capabilities to operate the FHSTs in other than a nominal condition. The following user-changeable parameters are associated with the star trackers:

- Misalignment of cameras
- Noises per camera per axis
- Biases per camera per axis
- Failures of individual cameras
- Guide stars per RFOV

- Additional stars per RFOV
- Number of RFOV per TFOV
- Number of scan lines per TFOV
- Methods for determining guide stars
- Size of TFOV per camera
- Size of RFOV per camera
- Star magnitude acceptability range
- Responds to normal ground commands

2.2 GROSS MODELING OF IRU

The IRU consists of three rate-integrating gyros and has six channels to measure angular displacement along the three spacecraft body axes. For each axis, one channel is primary and one is backup. For each channel, gyro data generation involves the following two steps: (1) calculating angular displacement and (2) modeling gyro noise to add onto the angular displacement. Angular displacement is calculated as follows:

1. Input angular spacecraft velocity vector, w.
2. Project w along channel input axis, G, to get rate, r, measured by that channel (r = G * w) in radians (rad)/sec.
3. Calculate angular displacement by integrating rate.

Gyro noise in GRO comes from two sources:

1. Noise on angular rate. This noise is modeled as Gaussian, zero mean, and white.
2. Noise on the rate of change of the gyro bias. This is noise modeled as Gaussian, zero mean, and white.

These noises are then added to the calculated gyro measurement and sent to the OBC as gyro data.

User-changeable parameters associated with the IRU are as follows:

- Misalignment of IRU
- Gyro rate bias
- Gyro drift

- Gyro drift rate
- Gyro and gyro channel failures

2.3 KALMAN FILTER

The Kalman filter is implemented in two steps. First, the propagation of the internal statistics based on the Dynamics Model and second, updating the state vector based on the Observation Model and the internal statistics.

2.3.1 DYNAMICS MODEL

The Dynamics Model for the GRO flight software Kalman filter is found in References 1 and 2. The gyro rate measurement is assumed to have the following form:

$$\dot{\theta} = w - b_o - b + n_v \qquad (1)$$

$$\dot{b} = n_u$$

where $\dot{\theta}$ = gyro rate measurement
w = true spacecraft rate
b_o = gyro bias
b = gyro drift bias
n_v = float torque noise (Gaussian white noise)
n_u = float torque derivative noise (Gaussian white noise)

Since b is the integral of a white noise, it becomes a random walk. The attitude rate error $\dot{\psi}$ is formed in the following manner:

$$\dot{\psi} = -b_o - b + n_v \qquad (2)$$

The gyro bias b_o is assumed to be known and can be derived from Equation (2). The Dynamics Model is then reduced to the following form:

$$\dot{\psi} = -b + n_v$$
$$\dot{b} = n_u \qquad (3)$$

If these two equations are put into a linear state space formulation, Equation (4a), Equation (4b) is derived:

$$\dot{X}(t) = F\,X(t) + W(t) \tag{4a}$$

$$\dot{X}(t) = \begin{bmatrix}\dot{\psi}\\ \dot{b}\end{bmatrix} = \begin{bmatrix}0_{3x3} & -I_{3x3}\\ 0_{3x3} & 0_{3x3}\end{bmatrix}\begin{bmatrix}\psi\\ b\end{bmatrix} + \begin{bmatrix}\eta_{v(3x1)}\\ \eta_{u(3x1)}\end{bmatrix} \tag{4b}$$

where ψ = attitude error
b = gyro drift bias
η_v = float torque noise (Gaussian)
η_u = float torque derivative noise (Gaussian)

$$E[W(t)] = 0$$

$$E[W(t)\,W^T(t')] = \begin{bmatrix}vI_{3x3}\,\delta(t-t') & 0_{3x3}\\ 0_{3x3} & uI_{3x3}\,\delta(t-t')\end{bmatrix} \tag{5}$$

$$Q(t) = E[W(t)\,W^T(t')]$$

where Q(t) is the spectral density matrix.

From Equation (4b) the state transition matrix $\Phi_k = \Phi(t_k, t_{k-1})$ is obtained, which allows one to solve for the dynamic noise covariance matrix, Q_k.

$$Q_k = \int_{t_{k-1}}^{t_k} \Phi(t_k,\tau)\,Q(\tau)\,\Phi^T(t_k,\tau)\,d\tau \tag{6}$$

$$P_k(-) = \Phi_k\,P_{k-1}(+)\,\Phi_k^T + Q_k \tag{7}$$

where $P_k(-)$ = propagated covariance matrix at time k
$P_{k-1}(+)$ = updated covariance matrix at time k-1

2.3.2 OBSERVATION MODEL

In the GRO flight software, the FHST measurements are used to create an observed star unit vector, OS, in the sensor coordinate frame. The identified star position in the star catalog is used to create an expected or computed unit star vector, CS, in the sensor coordinate frame. Then,

$$Z(i) = OS(i) - CS(i) \quad \text{for } i = 1 \text{ to } 2$$

where i = ith coordinate of the vectors
Z = measurement residuals

From this definition of Z, H is shown to be (Reference 3)

$$H_k = \begin{bmatrix} \left(\bar{X} \times \bar{S}_k\right)^T & 0 \\ \left(\bar{Y} \times \bar{S}_k\right)^T & 0 \end{bmatrix} \tag{8}$$

where S_k = observed star in spacecraft body frame
X = X coordinate of FHST in the spacecraft body frame
Y = Y coordinate of FHST in the spacecraft body frame

In the Observation Model

$$Z_k = H_k X_k + V_k \tag{9}$$

where Z_k = observation
V_k = sensor noise (Gaussian)

For sensor noise characteristics,

$$E[V_k] = 0 \tag{10}$$

$$E\left[V_k \; V_l^T\right] = \begin{bmatrix} R_{11} & 0 \\ 0 & R_{22} \end{bmatrix} \tag{11}$$

It is further assumed that the initial state vector X_o is Gaussian and X_o, W, and V_k are independent of each other. They all are assumed to be Gaussian, which is equivalent to assuming they are uncorrelated.

2.3.2 UPDATE ALGORITHMS

The state vector is updated by processing the following equation with the inputs $P_k(-)$ (Equation (7)), H (Equation (8)), R_k (Equation (11)), and the observation vector Z_k (Equation (9)).

$$K_k = P_k(-)\left[H_k^T \; H_k \; P_k(-) \; H_k^T + R_k\right]^{-1} \tag{12}$$

where K_k is the Kalman gain matrix.

$$P_k(+) = (I - K_k H_k) \; P_k(-) \tag{13}$$

where $P_k(+)$ is the updated covariance matrix.

$$X_k(+) = X_k(-) + K_k(Z_k - H_k X_k(-)) \tag{14}$$

where $X_k(+)$ is the updated state vector.

The GRO flight software employs a scaler implementation method that requires the sequence of Equations (12), (13), and (14) to be executed twice. In the first pass

$$\begin{aligned} H_k &= H_{k,1} = \left[\left(\bar{X} \times \bar{S}_k\right)^T \quad 0\right] \\ R_k &= R_{k,1} = R_{11} \end{aligned} \tag{15}$$

The resulting Kalman gain matrix $K_{k,1} = K_k$ is used to update the covariance matrix (Equation (13)) where $P_{k,1} = P_k$ and update the state (Equation (14)) where $X_k(-) = 0$. The equations are as follows:

$$K_{k,1} = P_k(-)\, H^T_{k,1} \Big/ \left[H_{k,1}\, P_k(-)\, H^T_{k,1} + R_{k,1}\right] \tag{16}$$

$$P_{k,1}(+) = [I - K_{k,1}\, H_{k,1}]\, P_k(-) \tag{17}$$

$$X_{k,1}(+) = K_{k,1}\, Z_1 \tag{18}$$

In the second pass, there are the following substitutions:

$$\begin{aligned} H_k &= H_{k,2} = \left[(\bar{Y} \times \bar{S}_k)^T \quad 0\right] \\ R_k &= R_{k,2} = R_{22} \\ K_k &= K_{k,2} \\ P_k(-) &= P_{k,1} \\ X_k(-) &= X_{k,1}(+) \end{aligned} \tag{19}$$

where $X_{k,1}(+)$ is the state vector update from the first pass.

The final Kalman gain matrix $K = K_{k,2}$ is used to update the covariance matrix $P_k(+) = P_{k,2}(+)$ and to update the state $X(+) = X_{k,2}(+)$. The equations are as follows:

$$K_{k,2} = P_{k,1}(+)\, H^T_{k,2} \Big/ \left[H_{k,2}\, P_{k,1}(+)\, H^T_{k,2} + R_{k,2}\right] \tag{20}$$

$$P_{k,2}(+) = [I - K_{k,2}\, H_{k,2}]\, P_{k,1}(+) \tag{21}$$

$$X_{k,2}(+) = X_{k,1}(+) + K_{k,2}\,[Z_2 - H_{k,2}\,X_{k,1}(+)] \tag{22}$$

$$X_k(+) = X_{k,2}(+), \qquad P_k(+) = P_{k,2}(+) \tag{23}$$

3. CASE STUDY OBJECTIVES AND IDENTIFICATION

There are three primary objectives in the case studies. First, the short-term stability and covariance of the Kalman filter are studied for a nominal baseline case. Second, the covariance and short-term stability of four cases involving sensor noise and misalignments are studied and compared with the baseline. Lastly, the short-term stability and covariance are studied for two anomalous cases.

The cases studied are as follows:

- Case 1: Baseline Simulation
- Case 2: Noise and Misalignment
  - 2A: Normal run with excessive gyro noise
  - 2B: Normal run with gyro unit misalignment
  - 2C: Normal run with excessive FHST noise
  - 2D: Normal run with FHST misalignment
- Case 3: Anomalous Simulations
  - 3A: One FHST with one and two guide stars
  - 3B: Convergence using one and two FHSTs

4. CASE STUDY RESULTS

The results described for each case were attained using two primary forms of data: statistical and Kalman error. A running mean and variance of the residuals from the OBC as well as other Kalman filter information were output to an analysis file that was read by a post-processor that produced plots and tabular data used for statistical analysis. The Kalman error is the error quaternion that represents the difference between the Truth Model state quaternion and the OBC state quaternion.

4.1 CASE 1: BASELINE SIMULATION

The nominal baseline case represents the expected on-orbit conditions for the spacecraft. Noises for this test case are based on latest values received from the manufacturers. The stability and statistics for the Kalman filter are based on a simulation of 90 minutes. The nominal noises for the sensor data are as follows:

- IRU float torque 0.20×10^{-6} radians (rad)/sec$^{3/2}$
  IRU float torque derivative 0.21×10^{-9} rad/sec$^{5/2}$
- FHST measurement noise 0.49×10^{-4} rad (10 arc-sec)

The Kalman error for this case is seen in Figure 2. The maximum error is in the roll axis, (R), where a bias of approximately 20 arc-sec can be observed. Both the pitch axis (P) and yaw axis (Y) show differences of less than 10 arc-sec. All three are well within the specified attitude determination requirement of 86 arc-sec (3 sigma).

Statistics for the baseline case measurement residuals are as follows:

Mean X (arc sec)	Mean Y (arc sec)
1.8	7.8

Mean X (rad)	Mean Y (rad)	Var X	Var Y
0.86×10^{-5}	-0.38×10^{-4}	0.23×10^{-8}	0.23×10^{-8}

The expected values for the residuals are zero. The baseline case shows the expected values of the measurements to be less than 10 arc-sec, which is the "zero reference" used for comparisons with other case studies.

4.2 CASE 2: NOISE AND MISALIGNMENT

4.2.1 CASE 2A: EXCESSIVE GYRO NOISE

The objective of this case is to identify unmodeled dynamic errors. Simulations were ran with the gyro noise of 5, 10, 20, and 50 times greater than the statistics modeled in the flight software Kalman filter. The excessive float torque and float torque derivative noise (Equation (4)) causes the filter to place too much weight on the Dynamics Model and eventually results in a divergence.

The Kalman errors shown in Figure 3 represent the worst case scenario (i.e., 50 times the nominal). It reveals no evidence of instability with the filter over the 90-minute simulation. However, the initial values of the Kalman error are larger than the baseline case but are quickly damped to within accepted values. This suggests that the Kalman filter is accurately accounting for the noise. The residual analysis (see Table 3), however, shows the divergence of the data with increasing noise. The mean of the X and Y residuals are approximately the same as the reference expected value in the baseline case. The variances though show an increased amount of excursion from the mean as the noise increases.

Table 3. Excessive Gyro Noise for Case 2A

Noise (X nominal)	Mean X (rad)	Mean Y (rad)	Var X	Var Y
1	0.86×10^{-5}	-0.38×10^{-4}	0.23×10^{-8}	0.23×10^{-8}
5	0.61×10^{-5}	-0.41×10^{-4}	0.37×10^{-8}	0.30×10^{-8}
10	0.82×10^{-5}	-0.43×10^{-4}	0.56×10^{-8}	0.43×10^{-8}
20	0.51×10^{-5}	-0.40×10^{-4}	0.16×10^{-7}	0.82×10^{-8}
50	0.12×10^{-5}	-0.38×10^{-4}	0.95×10^{-7}	0.39×10^{-7}

4.2.2 CASE 2B: MISALIGNMENT OF GYROS

In this case, the gyro assembly was misaligned 5 and 10 arc-sec. Table 4 lists the residual statistical results of this simulation, and the Kalman errors are plotted on Figure 4. Statistically, there is no observable difference. This is because the misalignment acts as a bias on the system that is too small to affect the system.

Table 4. Residual Statistical Results for Case 2B

Misalignment (arc sec)	Mean X (rad)	Mean Y (rad)	Var X	Var Y
5	0.68×10^{-5}	-0.41×10^{-4}	0.22×10^{-8}	0.27×10^{-8}
10	0.65×10^{-5}	-0.41×10^{-4}	0.22×10^{-8}	0.27×10^{-8}

4.2.3 CASE 2C: OBSERVATION NOISE

In this case, observation noise was added to one FHST and to both FHSTs. Tables 5 and 6 list the tabular statistical output for one FHST and two FSHTs, respectively. Figures 5 and 6 plot the Kalman errors for one FHST and two FHSTs, respectively. It can be seen from Figures 5 and 6 that the roll and pitch axis are biased when compared with the baseline simulation. Since the measurement data is being corrupted and the Kalman filter cannot extract the noise to produce a better measurement, the statistical data reflect the bias and divergence with increasing noise.

Table 5. Observation Noise With One FHST

Noise (X nominal)	Mean X (rad)	Mean Y (rad)	Var X	Var Y
5	0.76×10^{-5}	-0.73×10^{-4}	0.13×10^{-7}	0.17×10^{-7}
10	0.11×10^{-4}	-0.19×10^{-3}	0.51×10^{-7}	0.96×10^{-7}

Table 6. Observation Noise With Two FHSTs

Noise (X nominal)	Mean X (rad)	Mean Y (rad)	Var X	Var Y
5	0.27×10^{-4}	-0.21×10^{-3}	0.28×10^{-7}	0.66×10^{-7}
10	0.57×10^{-4}	-0.39×10^{-3}	0.11×10^{-6}	0.23×10^{-6}

4.2.4 CASE 2D: MISALIGNMENT OF FHST

This case simulated misaligning one FHST and both FHSTs. The effects did not show up in the residual statistics (Table 7), but they did appear in the Kalman filter errors (Figure 7).

Since the measurements were only biased, and misalignment is equivalent to biasing the measurement data, it is expected that the system would converge on the observed data with the same statistics as for the baseline. Also, with a bias in measurement data, it is expected that the Kalman error would converge to the biased value. From Figure 7, it can be seen that the roll-and-pitch-axes data converge to a biased point, whereas the yaw axis is equivalent to the baseline simulation. The roll axis and yaw axes data are 0.18×10^{-3} and 0.20×10^{-4} rad, respectively. A misalignment of 30 arc-sec in the FHST pitch axis is equivalent to 0.14×10^{-3} rad. Thus, the misalignment can be seen as a bias in the roll and pitch axes.

Table 7. Misalignment of FHST for Case 2D

Misalignment (arc sec)	Mean X (rad)	Mean Y (rad)	Var X	Var Y
One FHST 30	0.67×10^{-5}	-0.43×10^{-4}	0.17×10^{-8}	0.23×10^{-8}
Two FHSTs 30	0.4×10^{-5}	-0.37×10^{-4}	0.16×10^{-8}	0.23×10^{-8}

4.3 CASE 3: ANOMALOUS SIMULATIONS

4.3.1 CASE 3A: ONE FHST WITH ONE AND TWO GUIDE STARS

In this case, two subcases were studied: one FHST with one guide star and one FHST with two guide stars. The spacecraft did not maintain requirements with one FHST and one guide star. However, the spacecraft did maintain requirements for one FHST and two guide stars. Table 8 gives the residual statistics for both subcases, and Figures 8 and 9 give the Kalman filter attitude errors with one and two guide stars, respectively.

Table 8. Residual Statistics for Case 3A

Subcase	Mean X (rad)	Mean Y (rad)	Var X	Var Y
One Guide Star	0.12×10^{-4}	-0.51×10^{-5}	0.16×10^{-8}	0.11×10^{-8}
Two Guide Stars	0.21×10^{-4}	-0.91×10^{-5}	0.18×10^{-8}	0.12×10^{-8}

In the one-guide-star simulation, a large roll and pitch error divergence can be seen, whereas there is not a large yaw error divergence. An explanation can be found in looking at the LOS of the star being observed. No error will be detected if the spacecraft were to spin about this axis. Components of this revolution are in the roll and pitch axes of the spacecraft. However, a small movement in the yaw axis can be detected immediately.

In the two-guide-star simulation, the stars have an angular separation of 4.4 deg. If each star LOS is looked at separately, the preceding analogy is valid. However, since a break-track command is being sent every few minutes, the measurement data being used are alternated between the two stars. Thus, two observation vectors are available. This system is similar to the two-FHST configuration. The small angular separation between the star LOSs, as compared with the angular separation of the two FHSTs, requires a larger rotation angle to register a measurement error than does the two-FHST system.

4.3.2 CASE 3B: CONVERGENCE

This case tests the capability of recovering from a large error and converge within a required accuracy, providing the guide star is still within the TFOV. The case initializes the pointing error to 2.0 deg in the spacecraft body pitch axis. Initially, the spacecraft was at a -90-deg pitch. Two subcases are simulated for comparison. The first uses the normal configuration of two FHSTs, with one guide star per RFOV. The second involves one FHST and two guide stars. The convergence requirement for both cases is a Kalman error of $\leq$ 60 arc-sec (3 sigma). Figures 10 and 11 show the results of these two simulations for one guide star and two guide stars, respectively. With the nominal configuration, the 2.0-deg error was removed in approximately 22 minutes. The single FHST case took approximately 39 minutes to converge. The longer convergence time for the single FHST case was expected because of the small angular separation between star LOSs.

5. CONCLUSIONS

Five primary conclusions are derived from this study. First, the baseline simulation that contained expected on-orbit conditions performed within spacecraft specifications. Second, excessive dynamics noise (gyros) is picked up by the measurement residual statistics but not by the Kalman errors. Third, increasing observation noise is picked up by the measurement residual statistics and the Kalman errors are biased. These two results indicate that sensor failures can be picked up in the measurement residual statistics long before they show up in the Kalman errors. Fourth, misalignments for the gyros and FHSTs are picked up only in the Kalman errors. Lastly, convergence has been proven for the anomalous case of one FHST with two guide stars. The convergence required longer than the nominal two FHST with one guide star each simulation due to the small angles between observation vectors in one FHST.

REFERENCES

1. James W. Murrell, "Precision Attitude Determination for Multimission Spacecraft", AIAA Paper No. 78-1248, 1978

2. R. Farrenkopf, "Generalized Results for Precision Attitude Reference Systems Using Gyros," AIAA Paper No. 74-903, AIAA Mechanics and Control of Flight Conference, Anaheim, California, August 5-9, 1974

3. TRW, GRO Operations Data Book Part 3 - ACAD Subsystem, Volume II, 40420-86-322-001, September 2, 1986.

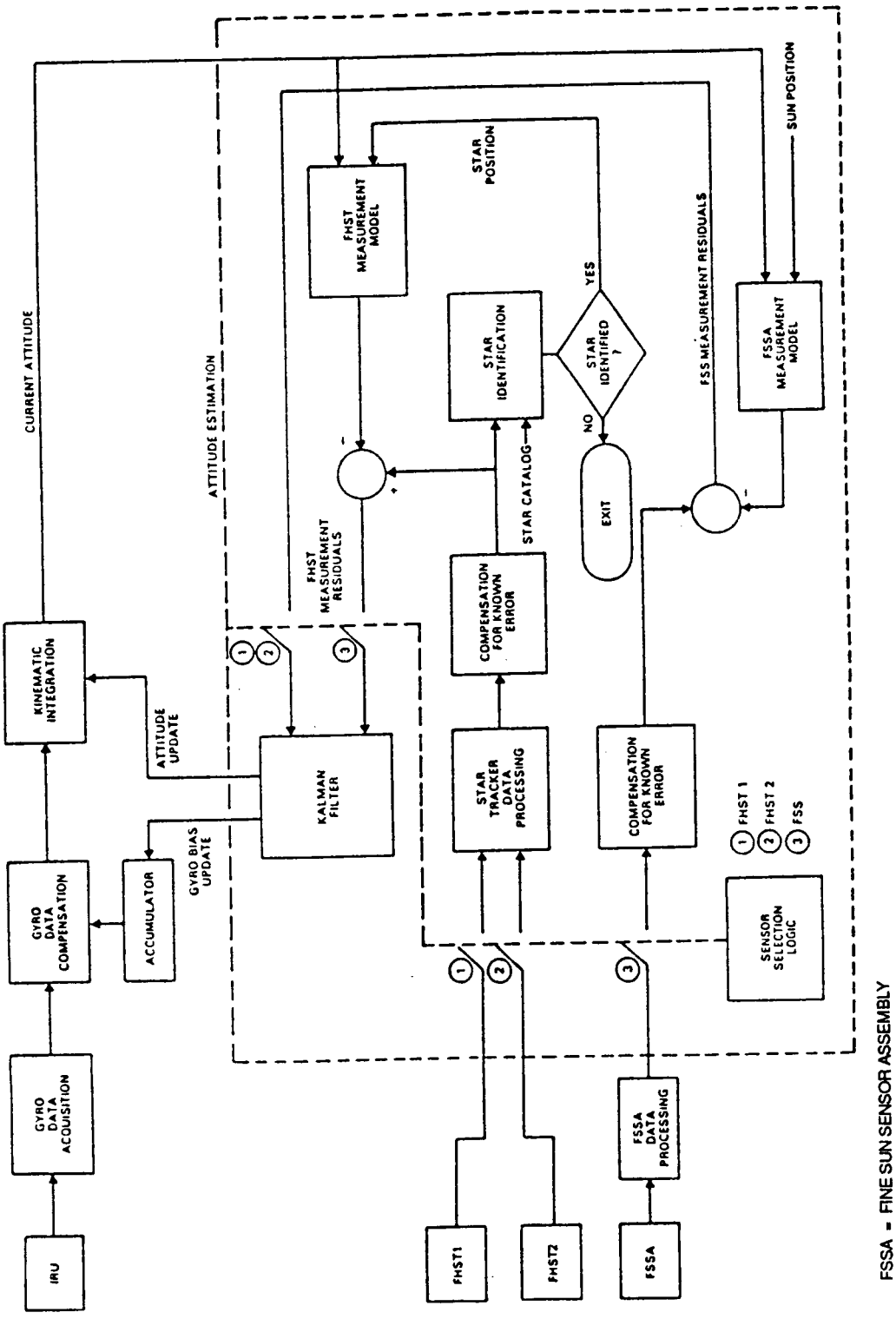

Figure 1. Attitude Estimation Algorithm Functional Block Diagram

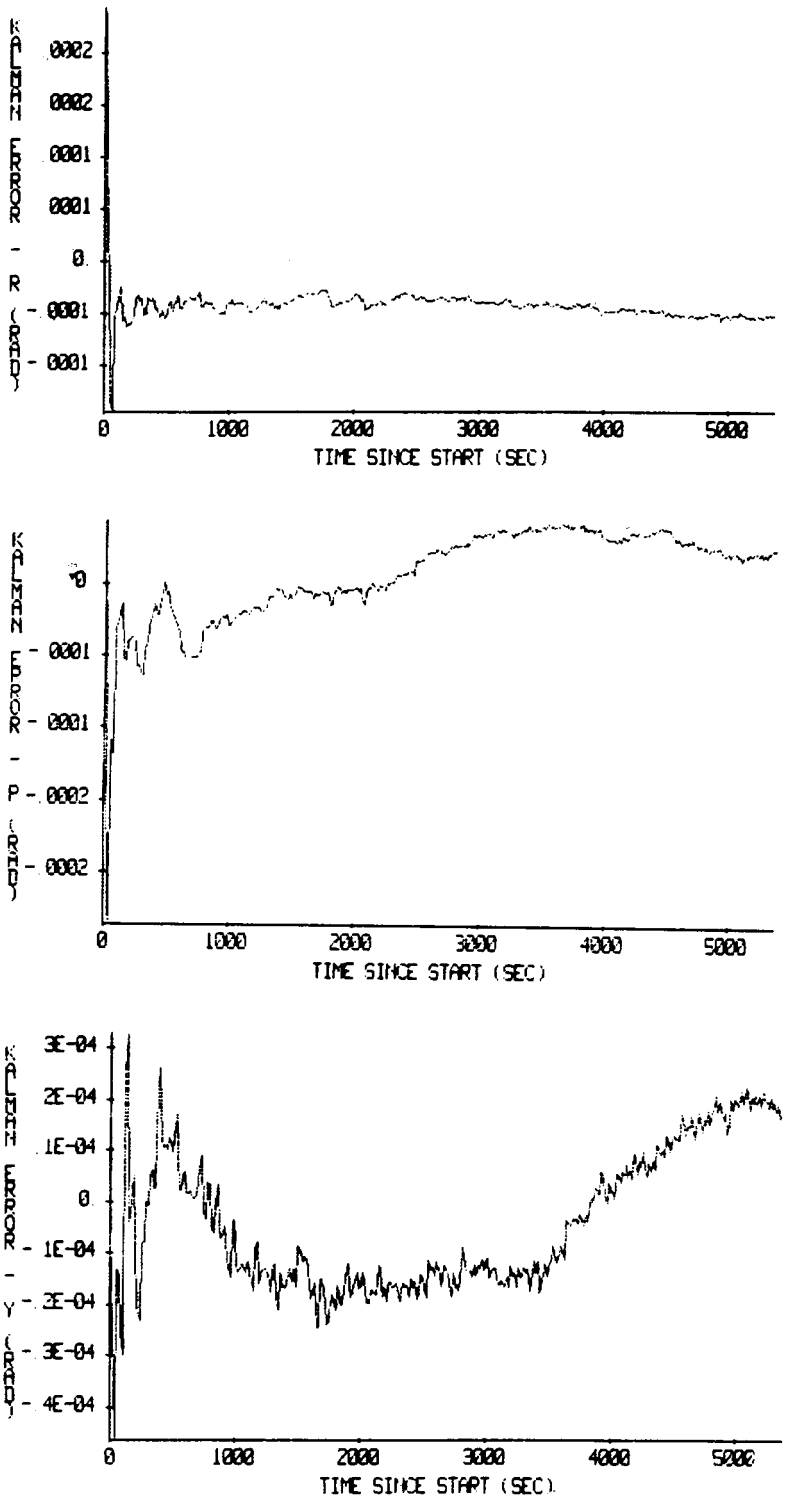

Figure 2. Baseline Nominal Performance

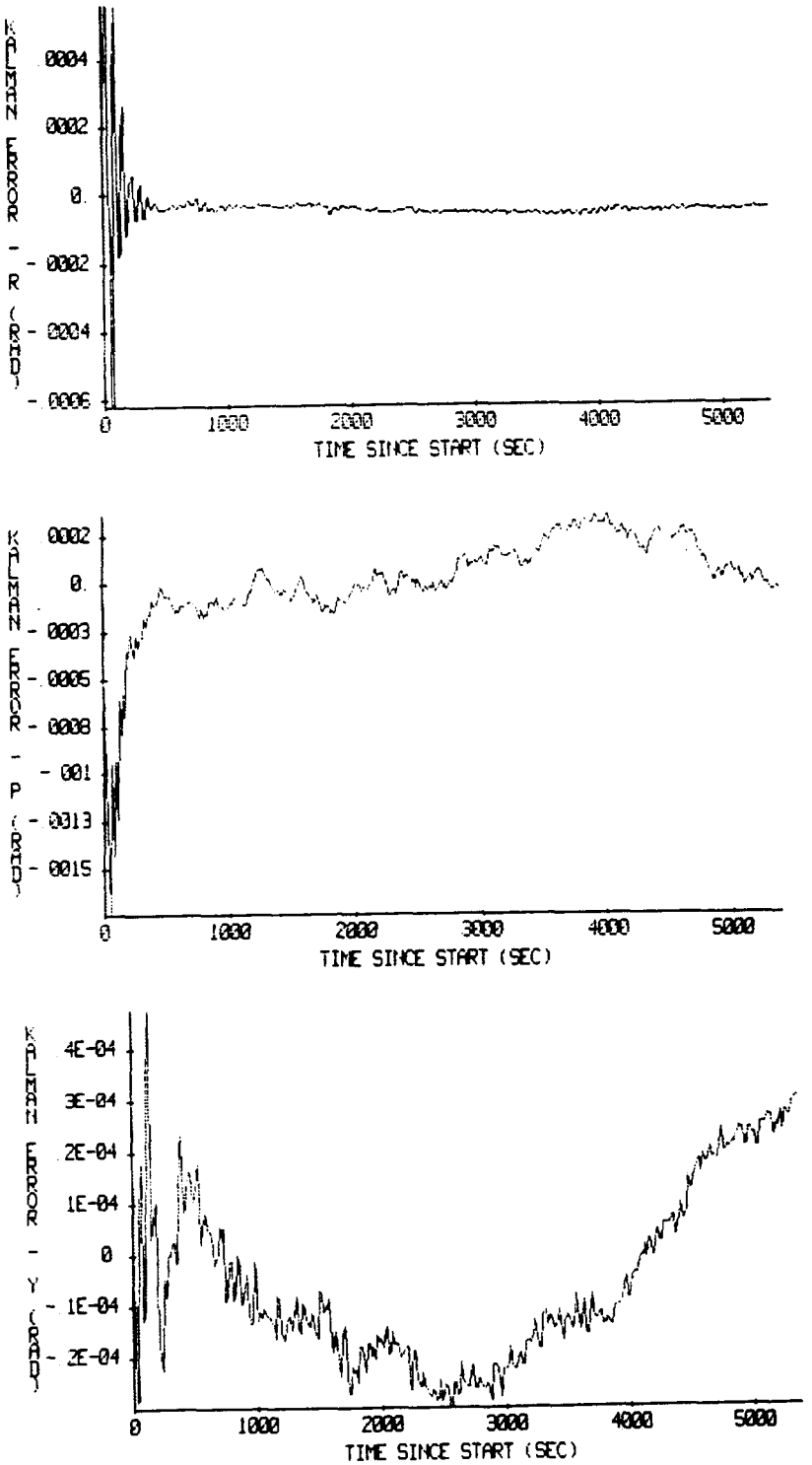

Figure 3. Modeling Noise on IRU

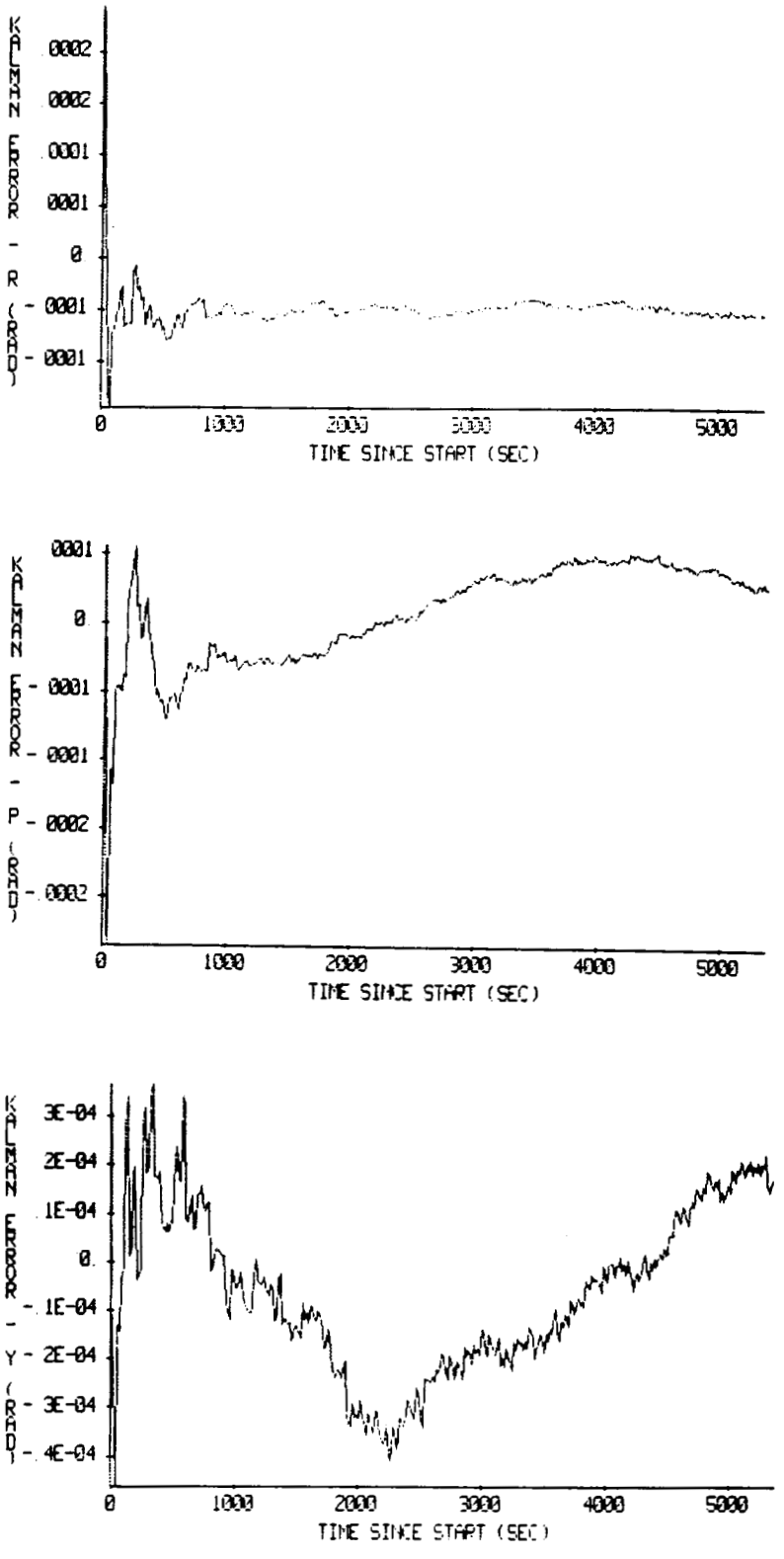

Figure 4. Misalignment of IRU

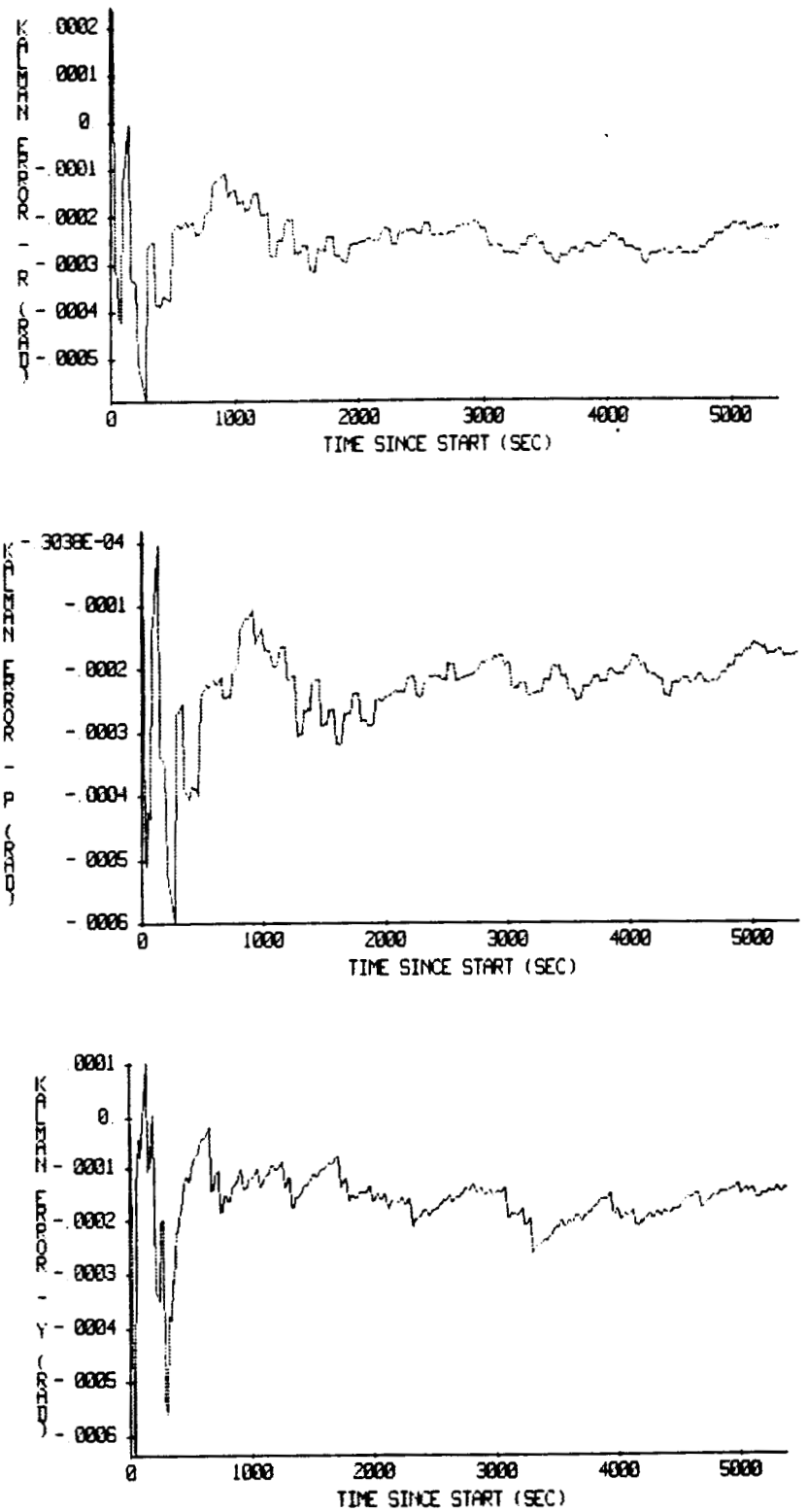

Figure 5. Observation Noise, One FHST

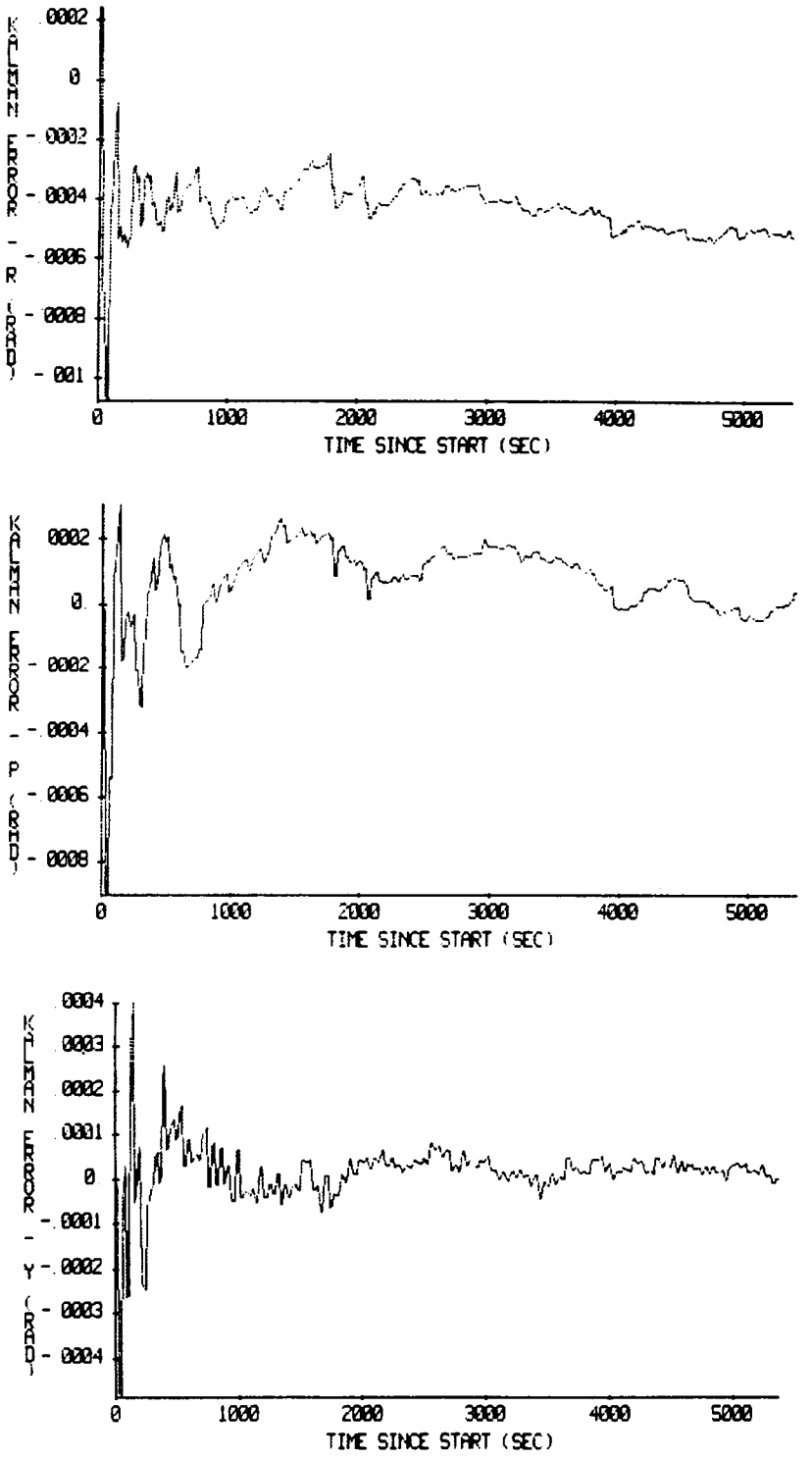

Figure 6. Observation Noise, Both FHSTs

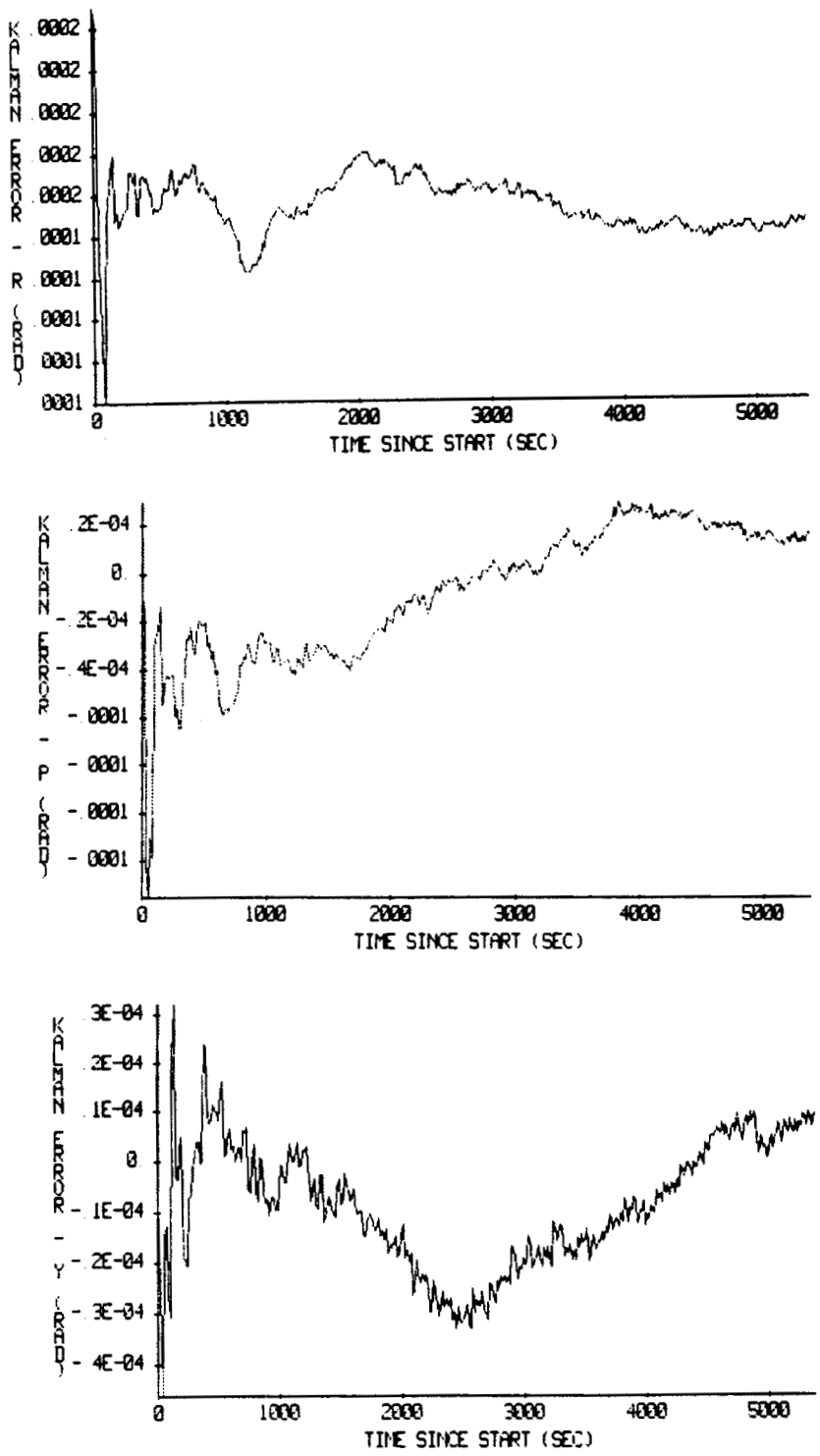

Figure 7. Misalignment, Both FHSTs

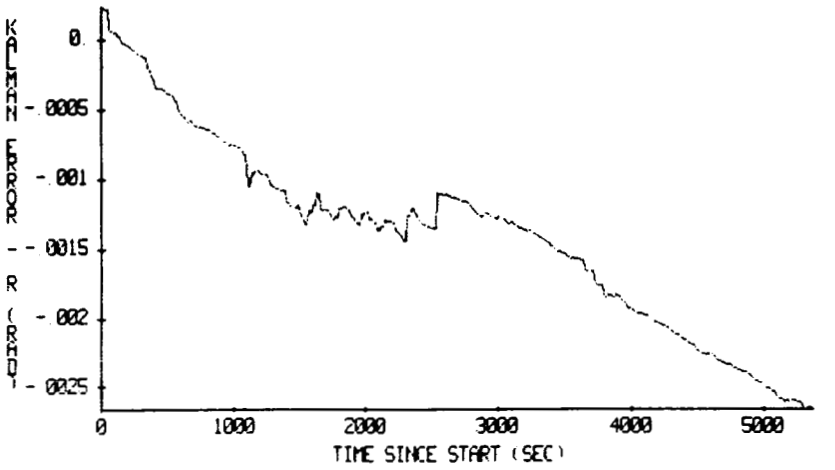

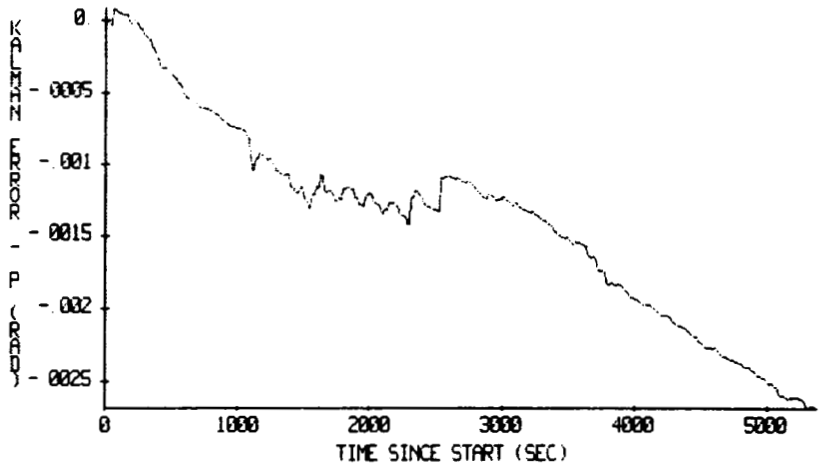

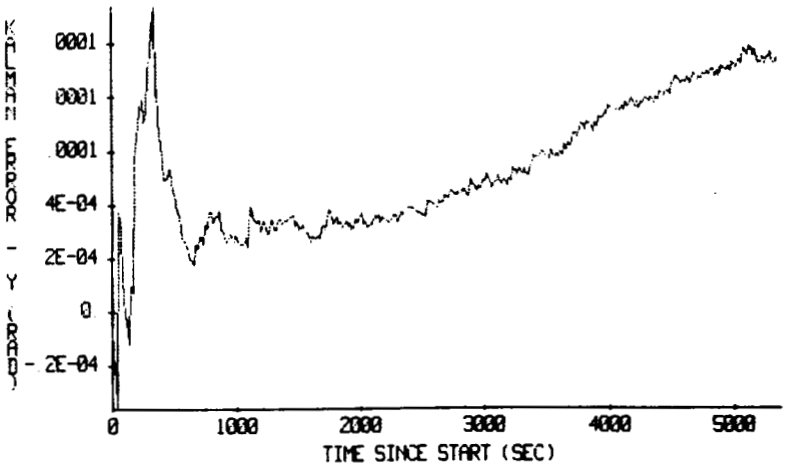

Kalman Filter Attitude Errors, One FHST and One Guide Star

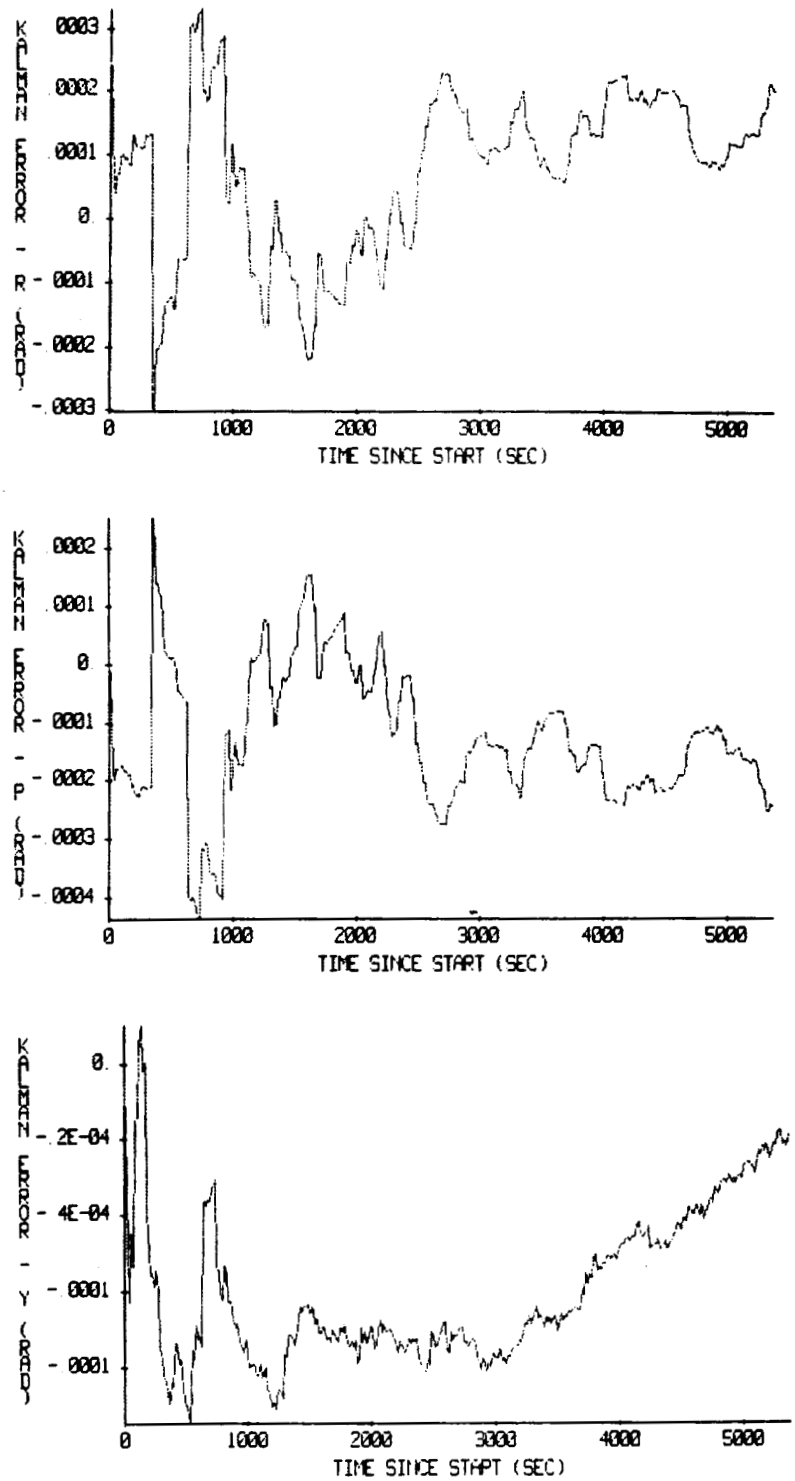

Figure 9. Kalman Filter Attitude Errors, One FHST and Two Guide Stars

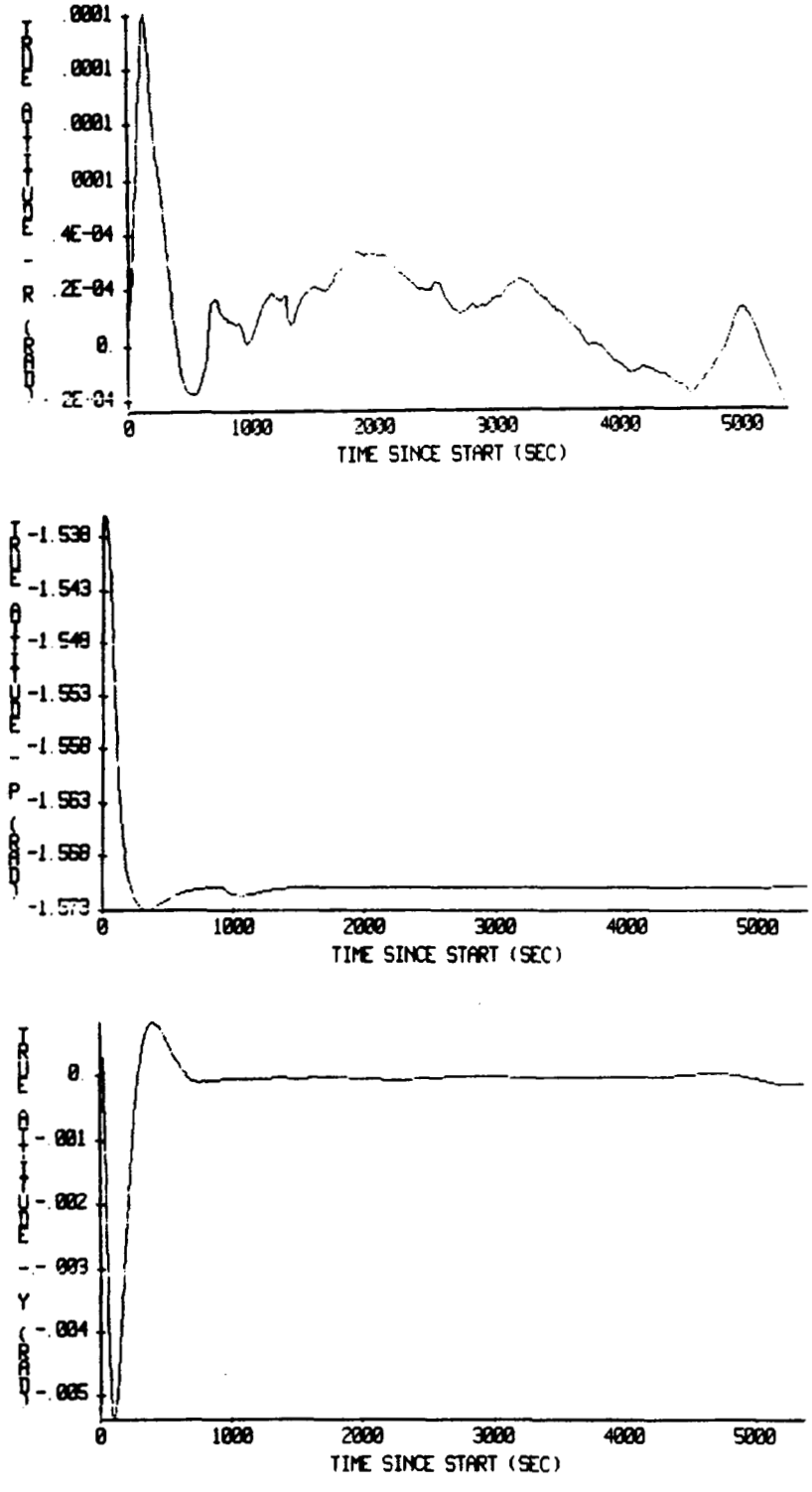

Figure 10. Both FHSTs, One Guide Star per FHST, and 2-deg Error in Pitch Axis

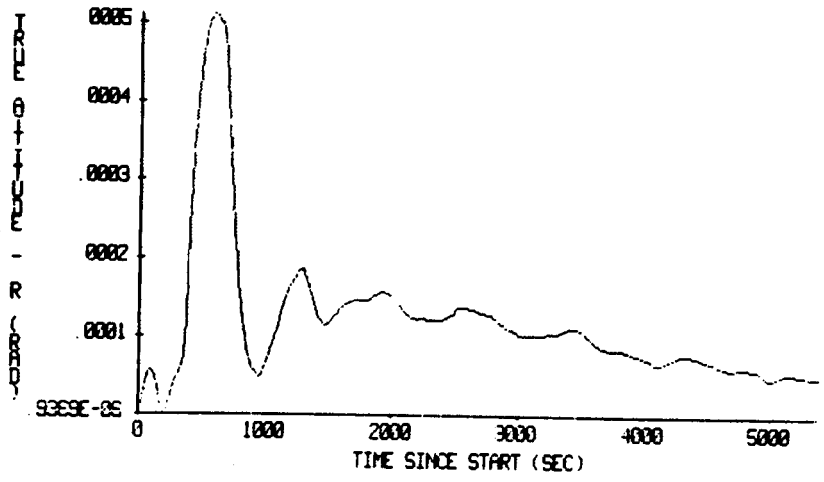

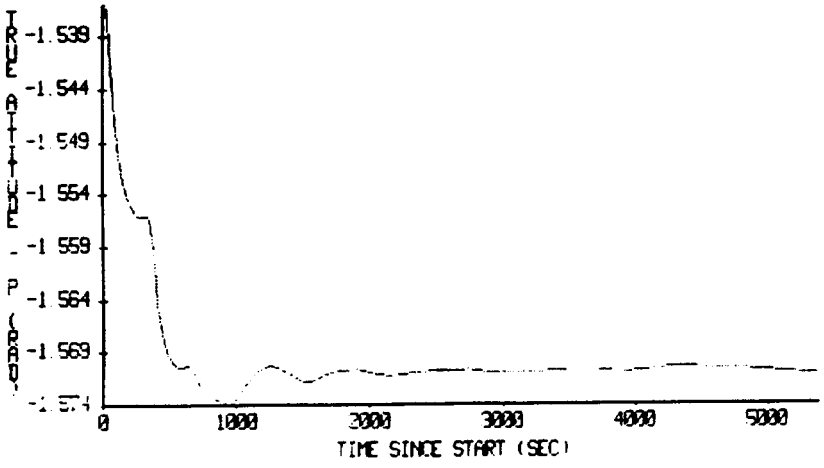

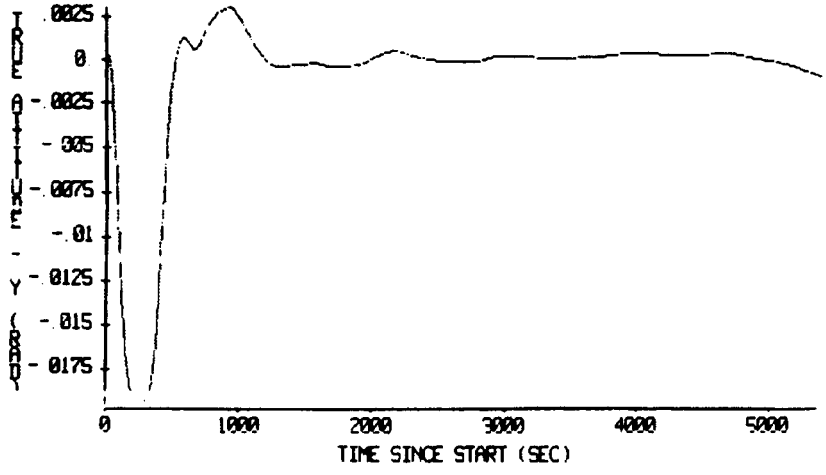

11. One FHST, Two Guide Stars, and 2-deg Error in Pitch Axis